The Astrophysical Journal Letters, 966:L15 (12pp), 2024 May 1 https://doi.org/10.3847/2041-8213/ad3ef5

Dark No More: The Low-luminosity Stellar Counterpart of a Dark Cloud in the Virgo Cluster*

Michael G. Jones[1], Steven Janowiecki[2], Swapnaneel Dey[1], David J. Sand[1], Paul Bennet[3], Denija Crnojević[4], Catherine E. Fielder[1], Ananthan Karunakaran[5,6], Brian R. Kent[7], Nicolas Mazziotti[1], Burçin Mutlu-Pakdil[8], and Kristine Spekkens[9,10]
[1] Steward Observatory, University of Arizona, 933 North Cherry Avenue, Room N204, Tucson, AZ 85721-0065, USA; jonesmg@arizona.edu
[2] University of Texas, Hobby–Eberly Telescope, McDonald Observatory, TX 79734, USA
[3] Space Telescope Science Institute, 3700 San Martin Drive, Baltimore, MD 21218, USA
[4] Department of Physics & Astronomy, University of Tampa, 401 West Kennedy Boulevard, Tampa, FL 33606, USA
[5] Department of Astronomy & Astrophysics, University of Toronto, Toronto, ON M5S 3H4, Canada
[6] Dunlap Institute for Astronomy and Astrophysics, University of Toronto, Toronto, ON M5S 3H4, Canada
[7] National Radio Astronomy Observatory, 520 Edgemont Road, Charlottesville, VA 22903, USA
[8] Department of Physics and Astronomy, Dartmouth College, Hanover, NH 03755, USA
[9] Department of Physics and Space Science, Royal Military College of Canada, P.O. Box 17000, Station Forces Kingston, ON K7K 7B4, Canada
[10] Department of Physics, Engineering Physics and Astronomy, Queen's University, Kingston, ON K7L 3N6, Canada

Received 2024 February 21; revised 2024 April 15; accepted 2024 April 15; published 2024 April 26

Abstract

We have discovered the stellar counterpart to the ALFALFA Virgo 7 cloud complex, which has been thought to be optically dark and nearly star-free since its discovery in 2007. This ~190 kpc long chain of enormous atomic gas clouds ($M_{\rm H\,I} \sim 10^9\,M_\odot$) is embedded in the hot intracluster medium of the Virgo galaxy cluster but is isolated from any galaxy. Its faint, blue stellar counterpart, BC6, was identified in a visual search of archival optical and UV imaging. Follow-up observations with the Green Bank Telescope, Hobby–Eberly Telescope, and Hubble Space Telescope demonstrate that this faint counterpart is at the same velocity as the atomic gas, actively forming stars, and metal-rich ($12 + ({\rm O/H}) = 8.58 \pm 0.25$). We estimate its stellar mass to be only $\log(M_*/M_\odot) \sim 4.4$, making it one of the most gas-rich stellar systems known. Aside from its extraordinary gas content, the properties of BC6 are entirely consistent with those of a recently identified class of young, low-mass, isolated, and star-forming clouds in Virgo that appear to have formed via extreme ram pressure stripping events. We expand the existing discussion of the origin of this structure and suggest NGC 4522 as a likely candidate; however, the current evidence is not fully consistent with any of our proposed progenitor galaxies. We anticipate that other "dark" gas clouds in Virgo may have similarly faint, star-forming counterparts. We aim to identify these through the help of a citizen science search of the entire cluster.

Unified Astronomy Thesaurus concepts: H I line emission (690); Virgo Cluster (1772); Galaxy interactions (600); Ram pressure stripped tails (2126); Star forming regions (1565)

1. Introduction

Surveys of atomic gas (H I) have a long history of identifying apparently dark structures made up of large quantities of neutral gas and (almost) no stars (e.g., Giovanelli & Haynes 1989; Chengalur et al. 1995; Verdes-Montenegro et al. 2001; Davies et al. 2004; Minchin et al. 2005; Haynes et al. 2007; Kent et al. 2007; Taylor et al. 2012; Wong et al. 2021; Józsa et al. 2022; Jones et al. 2023). H I is prone to forming such structures as it is typically the most loosely bound baryonic component of a galaxy's disk and is thus the most easily removed by external forces. Furthermore, as the distribution of H I often extends well beyond the stellar disk of a galaxy, it is relatively straightforward to strip gas, but no stars, thereby producing optically dark clouds.

Although some of the structures identified in the references above are still connected to their parent galaxies, some are detached, isolated, and apparently dark H I clouds with no clear point of origin. Such objects span several orders of magnitude in H I mass and are certainly not a single type of object. At high and intermediate masses, Kent et al. (2007) and Taylor et al. (2012) identified several dark H I clouds ($7 \lesssim \log M_{\rm H\,I}/M_\odot \lesssim 9$) in the direction of the Virgo cluster, and the Five-hundred-meter Aperture Spherical Telescope and the Green Bank Telescope (GBT) have recently identified lone H I clouds that may be ancient objects (Zhou et al. 2023; Karunakaran & Spekkens 2024; O'Neil et al. 2024). At the low-mass end, Adams et al. (2013) identified a sample of optically dark, compact H I clouds, some of which could be very low-mass halos in or near the Local Group.

When dealing with H I-only detections of local objects (e.g., $cz \lesssim 5000$ km s^{-1}), it is challenging to determine accurate distances, and these systems may not be as they first appear. Adams et al. (2015), Bellazzini et al. (2015), and Sand et al. (2015) all, almost simultaneously, realized that one of the Adams et al. (2013) objects (AGC 226067) did contain a small number of stars and was ~10× farther away and ~100× more massive than first thought. This object, now commonly referred to as SECCO 1, was found to be an isolated pocket of recent star

---

* Based on observations obtained with the Hobby–Eberly Telescope (HET), which is a joint project of the University of Texas at Austin, the Pennsylvania State University, Ludwig-Maximillians-Universitaet Muenchen, and Georg-August Universitaet Goettingen. The HET is named in honor of its principal benefactors, William P. Hobby and Robert E. Eberly.

formation (SF) embedded in the hot intracluster medium (ICM) of the Virgo cluster. Its rich metallicity (Beccari et al. 2017) and exclusively young stellar population (Sand et al. 2017) indicated that it must have formed recently from stripped gas, but there was no candidate parent galaxy within over 200 kpc.

Sand et al. (2015) searched for other objects with similar optical and UV morphology to SECCO 1, identifying five additional candidates in Virgo. With Hubble Space Telescope (HST) imaging, plus Jansky Very Large Array (VLA), GBT, and Multi Unit Spectroscopic Explorer observations (Jones et al. 2022a, 2022b; Bellazzini et al. 2022), we demonstrated that four[11] of these are analogous to SECCO 1 (though not all are H I-rich) and argued that they represent a new class of object, which we will refer to simply as "blue blobs." The only viable mechanism to explain both the isolation and young ages of blue blobs is high-speed ram pressure stripping of H I-bearing galaxies falling into the cluster (Jones et al. 2022b). Even so, it is remarkable that they survived traversing hundreds of kpc through the hot ICM and may be the first examples of isolated star-forming clouds supported (in part) by external pressure (Burkhart & Loeb 2016; Bellazzini et al. 2018; Calura et al. 2020; Jones et al. 2022b).

With the goal of better understanding the population statistics of these new objects, we embarked on a uniform search for candidates covering the entire cluster (described in Section 2). When we began following up our initial candidates (Section 3), one (known as Blue Candidate 6, BC6) was found to be coincident (both in position and velocity) with the largest of the "dark" H I cloud complexes identified by Kent et al. (2007), ALFALFA Virgo 7. In a follow-up investigation, Kent et al. (2009) found that VCC 1357 overlaps with this H I structure but was deemed to likely be in projection and not physically associated with the gas due to its color and dwarf spheroidal morphology. Another faint coincident object was noted by Kent et al. (2009), but more recent imaging clearly indicates that this is a distant background group of galaxies. Thus, no convincing stellar counterpart had been identified for this H I structure since its discovery. Here we show (Section 4) that ALFALFA Virgo 7 has a definite stellar counterpart that is over 20,000 times less massive than the H I and is made up exclusively of stars that recently formed in situ. The stellar properties of this object closely match those of the recently identified blue blobs (Jones et al. 2022b). BC6 differs only in its exceptional H I content. In Section 5, we discuss the potential point of origin of this object and its likely fate. We present our conclusions in Section 6.

Throughout this Letter, we attempt to use "BC6" to refer to the stellar component that we have identified and the "H I cloud complex" to refer to the (previously dark) H I structure identified by Kent et al. (2007). We also assume throughout that BC6 and the associated H I complex are in the Virgo cluster at a distance of 16.5 Mpc (Mei et al. 2007). We note that this assumption is consistent with all observations, in particular the color–magnitude diagram (CMD; Sections 3.4 and 4.1).

2. Identification of Candidates

The blue blob candidates presented in Jones et al. (2022b) arose from a cursory search (Sand et al. 2015) of the Virgo cluster, and there are likely additional examples. In an attempt to identify additional objects, we began a visual search of the available imaging within the cluster from the Next Generation Virgo cluster Survey (NGVS; Ferrarese et al. 2012), the Dark Energy Camera Legacy Survey (DECaLS; Dey et al. 2019), and the Galaxy Evolution Explorer (GALEX; Martin et al. 2005). A full description of this search will be presented in S. Dey et al. (2024, in preparation); here we provide a brief summary.

Matching $3' \times 3'$ image cutouts from the three surveys were produced, covering the full area of the NGVS. The DECaLS *gri* color images were taken directly from the Legacy Surveys Viewer,[12] as were the GALEX near-UV (NUV) + far-UV (FUV) images. In the case of NGVS, we produced our own color images from the *u*, *g*, and *i* filters, with a stretch designed to bring out faint, blue features (saturating most normal galaxies in the cluster). These image cutouts were uploaded to the `Zooniverse` website, where team members (primarily M. Jones, S. Dey, and D. Sand) searched for objects that had UV emission (or were exceptionally blue in the optical) but extremely faint, irregular, and clumpy appearances in the optical images.[13]

The most compelling blue blob candidates to emerge from this search, one of which was BC6 (Figure 1), were selected for follow-up observations with GBT, HST, and the Hobby–Eberly Telescope (HET) to search for H I gas content, resolve their stellar populations, and search for optical emission lines, respectively. These observations are discussed in Section 3.

3. Observations

BC6 lies in the direction of the Virgo cluster approximately 2°.7 S of M87 and 1°.7 N of M49, that is, roughly halfway between the Virgo A and B clouds (Binggeli et al. 1987). Typical cluster members in this direction have line-of-sight velocities in the range $850 \lesssim cz/\mathrm{km\,s^{-1}} \lesssim 1200$, but the scatter is several hundred $\mathrm{km\,s^{-1}}$ beyond either side of this range (Mei et al. 2007). There is a bridge of diffuse X-ray emission that connects M87 to M49 (Böhringer et al. 1994), indicating that the hot ICM is of higher density in this region than would be expected given its separation from the cluster core. BC6 lies roughly on this bridge.

3.1. NGVS, DECaLS, and GALEX

BC6 appears to have three main components (Figure 1). The largest and brightest is just S of a background galaxy that is visible in both optical and UV images. This main component (BC6a) contains a bright knot of FUV emission (blue in Figure 1, right) and appears as a faint, clumpy, blue smudge in the NGVS image. The other two components are even fainter and are to the NE and E of the brightest component. BC6b (to the NE) has faint but still clearly discernible UV emission, while BC6c (to the E) is barely detected in UV and appears only as a few blue points in the NGVS image.

Aperture photometry was performed on the NGVS *g* and *i* filters and GALEX NUV using the Aperture Photometry Tool (Laher et al. 2012). Due to the irregular morphology of BC6, elliptical apertures were manually tailored for each component,

---

[11] The fifth object is resolved as a background galaxy group in HST imaging (Jones et al. 2022b).

[12] www.legacysurvey.org/viewer

[13] This initial search has since evolved into a full citizen science project that will be presented in detail in S. Dey et al. (2024, in preparation) and N. Mazziotti et al. (2024, in preparation). It is available at https://www.zooniverse.org/projects/mike-dot-jones-dot-astro/blobs-and-blurs-extreme-galaxies-in-clusters.

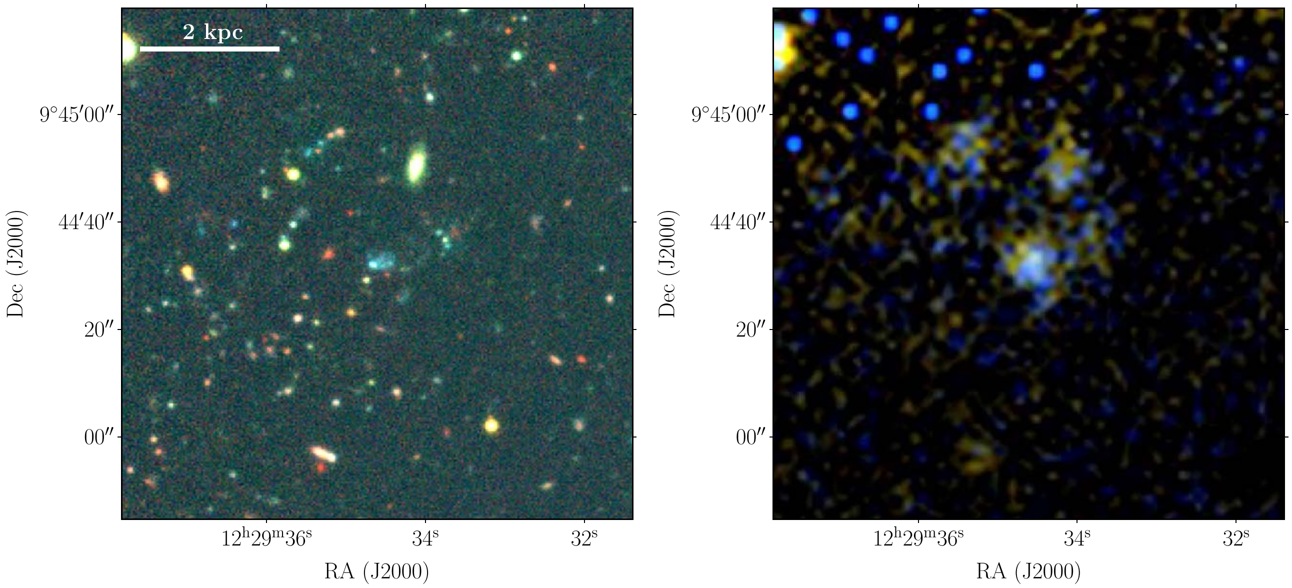

Figure 1. Left: NGVS *ugi* image of BC6, similar to the image in which it was originally identified. Right: GALEX NUV+FUV image similar to that used for the original identification and covering the same field as in the left panel. The source is deliberately unlabeled, but its components are circled in Figure 3 (right), which shows a similar field of view. Without the comparison of the optical and UV images, blue blobs would be almost impossible to identify. The bright blue speckles in the top left of the right panel are an artifact from the GALEX FUV data.

Table 1
Properties of BC6

Parameter	Value
R.A. (J2000)	12:29:35
decl. (J2000)	+9:44:32
$v_{\mathrm{H}\alpha}$ (km s^{-1})	500 ± 4
m_g (mag (AB))	21.01 ± 0.15
m_i (mag (AB))	21.16 ± 0.40
m_{F606W} (mag (AB))	20.69 ± 0.15
m_{F814W} (mag (AB))	20.94 ± 0.37
M_V (mag (AB))	−10.4
$\log L_V$ ($L_\odot$)	6.05
$\log(\mathrm{SFR}_{\mathrm{NUV}}/M_\odot\ \mathrm{yr}^{-1})$	−3.51 ± 0.04
$\log(\mathrm{SFR}_{\mathrm{H}\alpha}/M_\odot\ \mathrm{yr}^{-1})$	−4.36 ± 0.13
$12 + \log(\mathrm{O/H})_{\mathrm{O3N2}}$	8.58 ± 0.25
$\log M_*$ ($M_\odot$)	∼4.4

Note. Absolute quantities assume a distance of 16.5 Mpc.

and the median sky level was subtracted based on annuli beyond them. Galactic extinction was corrected using the dust maps of Schlegel et al. (1998) and the filter coefficients from Wyder et al. (2007) and Schlafly & Finkbeiner (2011). Using standard conversions (Iglesias-Páramo et al. 2006; Morrissey et al. 2007), we converted the GALEX NUV flux into an SF rate (SFR) estimate. These photometry values are listed in Table 1.

3.2. GBT

After the identification of BC6 and several other candidates in the NGVS and GALEX imaging, we rapidly embarked on a follow-up program with a joint GBT–HST project, GBT-22B-080 (PI: M. Jones), to search for H I gas in all candidates and to obtain high-resolution imaging of the stellar population of BC6. In addition, we followed up candidates with an HET project (PI: S. Janowiecki) to obtain optical spectroscopy of nebular emission lines (Section 3.5).

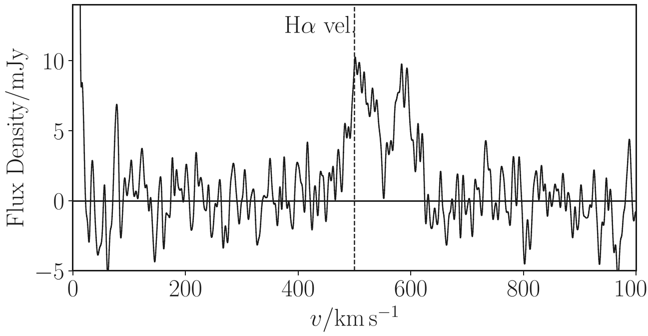

Figure 2. GBT H I spectrum at the location of BC6. The vertical dashed line indicates the velocity of BC6 determined from Hα line emission (Section 3.5). The profile is double horned because the large GBT beam includes some emission from the adjacent H I cloud just to the SE (denoted as C4 by Kent et al. 2009), which is at a slightly higher velocity.

Before it was realized that BC6 was the stellar counterpart to the H I structure identified by Kent et al. (2007), and that it therefore already had H I observations, it was included as a target in the GBT project. BC6 was observed in 2023 April with six 10 minute on/off integrations with the Versatile GBT Astronomical Spectrometer backend. The data were reduced using standard procedures in `GBTIDL`.[14] After smoothing to a spectral resolution of 5 km s^{-1}, the resulting spectrum (Figure 2) has an rms noise of 1.77 mJy. H I line emission is strongly detected in the 9′.1 GBT beam along the BC6 line of sight between 475 and 625 km s^{-1}.

3.3. ALFALFA

The Arecibo Legacy Fast ALFA (Arecibo *L*-band Feed Array), or ALFALFA, survey (Giovanelli et al. 2005; Haynes et al. 2011, 2018) mapped approximately 3000 deg^2 of the sky

---

[14] https://gbtidl.nrao.edu

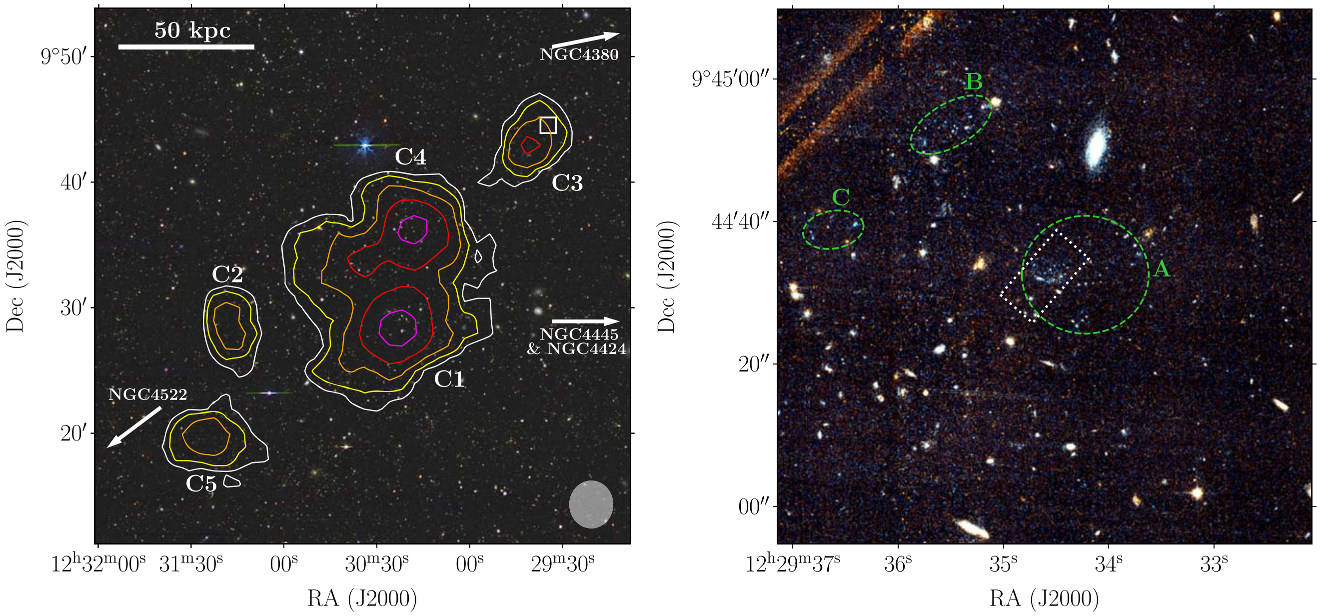

Figure 3. Left: ALFALFA H I contours overlaid on a *griz* DECaLS image. BC6 is coincident with a cloud at the NW tip of the H I complex (and is at the same velocity; see Figure 2). The five component clouds of the H I complex are labeled C1–5 as in Kent et al. (2009). The white box (inside cloud C3) indicates the location of BC6 and shows the size of the field of view of the HST image (right panel). The lowest H I column density contour level is 2.2×10^{18} cm^{-2} (over 20 km s^{-1}), and each subsequent contour is double the previous. The ALFA beam size is shown in the bottom right corner. The white arrows around the edge of the panel indicate the directions toward some of the neighboring galaxies discussed in Section 5.1 and Table 3. Right: HST ACS F814W+F606W color image of BC6. The three components are circled with dashed green ellipses. These are the regions used to produce the CMD of BC6 (Figure 4). The white dotted rectangle indicates the region targeted with HET/LRS2-B.

for H I line emission, including the Virgo cluster. Kent et al. (2007) originally identified the H I cloud complex in a preliminary ALFALFA data set. These data have a channel width of ∼5 km s^{-1}, a pixel size of 1′, and a spatial resolution of approximately $3\farcm8$. We created our own version of the moment zero map of the H I emission in the cloud complex using the `SoFiA` (Serra et al. 2014, 2015) masking tool, adopting the standard smooth and clip algorithm with spatial smoothing kernels of $4\farcm0$ and $8\farcm0$, with both no spectral smoothing and smoothing over two and four channels (∼10 and ∼20 km s^{-1}). We set a detection threshold of 3.5σ in order to include relatively faint emission but coupled this with a high reliability threshold (95%) in order to ensure that only sources that are high signal-to-noise ratio (S/N) overall were retained. The moment zero map of the emission included in the `SoFiA` mask is shown in Figure 3 (left) as contours on a DECaLS optical image.

We estimate the H I mass of the entire structure by integrating all of the flux within the `SoFiA` mask and assuming a distance of 16.5 Mpc. This gives a value of $\log(M_{\rm H\,I}/M_{\odot}) = 8.83 \pm 0.04$. We note that this is about 0.1 dex higher than the value in Kent et al. (2009). However, in that work, they considered each cloud component as a separate source, which may have led to some extended flux being missed, whereas `SoFiA`'s spatial and spectral smoothing improves our ability to recover extended emission. In addition, Minchin et al. (2019) used deeper Arecibo observations to estimate a total H I mass of $\log(M_{\rm H\,I}/M_{\odot}) = 9.1$, arguing that the additional flux (compared to ALFALFA) comes from low column density extended emission.[15]

3.4. HST Imaging

HST Advanced Camera for Surveys (ACS) images of BC6[16] were taken in 2023 February as part of the program GO-17267 (PI: M. Jones). The imaging used the Wide Field Channel of ACS with the F606W and F814W filters. Over the course of two orbits, four exposures were taken in each filter, resulting in total integration times of approximately 2000 s in F606W and F814W. A false-color composite of these images is shown in Figure 3 (right), centered on BC6.

Point-source photometry was carried out with `DOLPHOT` (Dolphin 2000, 2016), which uses the Vega magnitude system. Thus, our point-source photometry is in the Vega system. Quality cuts to eliminate unwanted sources (e.g., background galaxies and diffraction spikes) were made as described in Section 3.1 of Jones et al. (2022b). Artificial star tests were used to estimate the 90% and 50% completeness limits of the source catalog (as in Jones et al. 2022a). The `Python` package `dustmaps` (Green 2018) was used to correct the point-source photometry for Galactic extinction using the maps of Schlegel et al. (1998) and the coefficients from Schlafly & Finkbeiner (2011) for the F606W and F814W filters. The typical extinction was very minor, with a mean $E(B-V)$ value of 0.024 mag. Stars within the ellipses in Figure 3 (right) are shown in the CMD in Figure 4. A background CMD is also shown for an equal area region far from BC6.

In addition to the point-source photometry, we also performed aperture photometry on the HST images in order to measure the integrated magnitude of BC6 in the F606W and F814W filters. To do this, we used the drizzled images in each filter and the apertures plotted in Figure 3 (right). Owing to the highly irregular morphology of BC6, these apertures were

---

[15] Minchin et al. (2019) also applied a 33% (0.1 dex) correction factor to account for the Arecibo/ALFA side-lobe response. Both Kent et al. (2009) and Minchin et al. (2019) adopt a distance of 16.7 Mpc for Virgo, which would increase their mass estimates by 2.4% (0.01 dex) relative to ours.

[16] DOI:10.17909/h12e-gb42

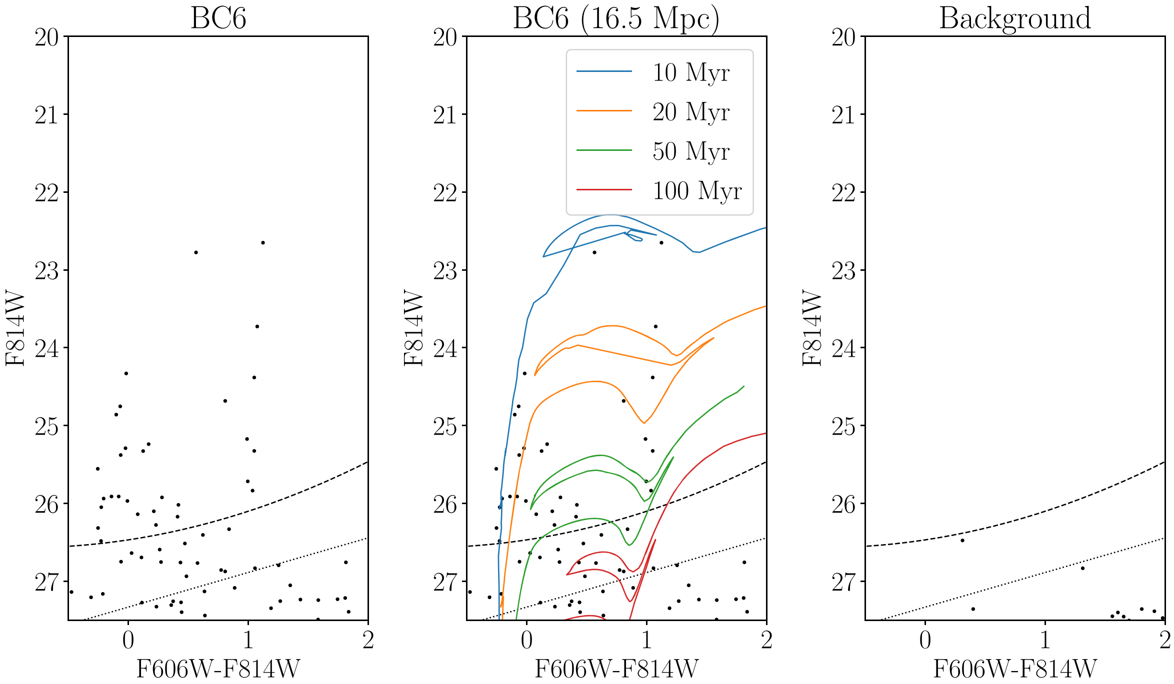

Figure 4. Left: CMD of BC6 within the regions shown in Figure 3 (right). Center: the same CMD with PARSEC isochrones for stellar populations with ages between 10 and 100 Myr. All isochrones have a metallicity of [M/H] = −0.1, roughly matching that measured from emission lines (Table 2), and are scaled to an assumed distance of 16.5 Mpc. Right: CMD of a blank sky region (equal in area to the sum of the apertures in the left panel) of the HST image away from the target. In all panels, the dashed curved line indicates the 90% completeness limit, and the straight dotted line is the 50% limit. All magnitudes are in the Vega system and corrected for Galactic extinction.

manually constructed to encompass the regions containing blue stars and UV emission, as well as the distribution of light in the NGVS image (Figure 1, left). Using the `Photutils` (Bradley et al. 2020) package, the integrated magnitude within these apertures was measured and the background contribution subtracted based on the median sky value within annular apertures around each component. For comparison purposes, we also convert to an absolute *V*-band magnitude based on Sirianni et al. (2005) and an assumed distance of 16.5 Mpc. These magnitude measurements are quoted in Table 1.

3.5. HET Optical Spectroscopy

We observed the main component of BC6 (the largest ellipse in Figure 3, right) with the blue spectrograph of the Low Resolution Spectrograph 2 (LRS2-B; Chonis et al. 2016) on the 10 m HET (Ramsey et al. 1998; Hill et al. 2021) under clear dark skies on the night of 2023 April 19 with a 3300 s exposure. The LRS2-B has $R \approx 1100$ and an integral field unit that is $6'' \times 12''$ with $0\farcs6$ lenslet fibers on sky, giving an abundance of sky fibers around the relatively compact optical emission from BC6. We use the Hα line to determine which spaxels include emission from BC6 and extract all spaxels within $1\farcs5$ of the peak of the source with the `LRS2Multi` extension to the `Panacea` data reduction pipeline.[17] Briefly, this data reduction includes the necessary detector characterizations, fiber extraction, wavelength calibration, mirror illumination correction, sky subtraction, and 1D spectral source extraction, including a treatment of differential atmospheric refraction in the sky and object spectra. The resulting spectrum is shown in Figure 5.

The spectrum is fairly typical of an H II region, with clear, albeit relatively weak, emission lines. Only the Hα line is of high enough S/N to be fit with a Gaussian. Thus, this line alone was used to determine the redshift $cz = 500 \pm 4$ km s^{-1} (with a barycentric correction applied). To obtain fluxes from the other lines, we extract the integrated signal within a $\pm 2\sigma_{\mathrm{H}\alpha}$ region centered on the redshifted wavelength on each line. Here $\sigma_{\mathrm{H}\alpha}$ is the standard deviation of the Gaussian profile fit to the Hα line. Flux errors are estimated by summing the uncertainty values in the same wavelength range and dividing by the square root of the number of channels included.

A reddening correction was calculated by assuming an intrinsic value of Hα/Hβ = 2.87 (for an H II region at 10^4 K; Osterbrock 1989), an R_V value of 3.1, and the Fitzpatrick (2004) extinction law. Based on the observed line ratio Hα/Hβ = 3.28, we calculated an extinction value of $E(B-V) = 0.11$. This suggests that there is some internal extinction within BC6, as the Schlegel et al. (1998) dust map in this direction indicates minimal Galactic extinction ($E(B-V) \approx 0.02$). Observed line fluxes were corrected for extinction (using the extinction model of Fitzpatrick 2004) implemented in the `Python` package `dust_extinction`.[18] These fluxes and uncertainties are provided in Table 2. For consistency, the quoted Hα flux does not correspond to that calculated with the Gaussian fit but is instead calculated in the same manner as the other lines.

We note here that the $E(B-V) = 0.11$ extinction estimate is, strictly speaking, only applicable to the H II region, as it is likely the result of dust in its immediate vicinity. For simplicity, we apply the Galactic extinction correction only for all stars in the HST CMD (Section 3.4 and Figure 4), even though for a

---

[17] https://github.com/grzeimann/LRS2Multi and https://github.com/grzeimann/Panacea

[18] https://dust-extinction.readthedocs.io

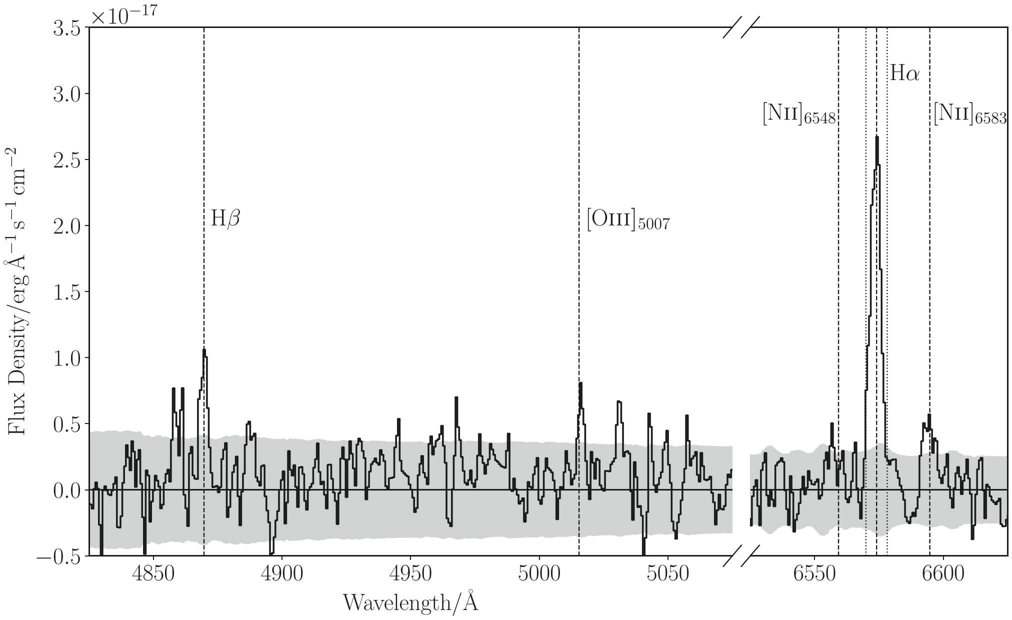

Figure 5. HET LRS2-B spectrum of BC6 showing the Hα, Hβ, [N II], and [O III] lines. The marked wavelengths of each line (vertical dashed lines) are all shifted to match the redshift of Hα. The vertical dotted lines indicate ±2 standard deviations of the Gaussian fit to the Hα line. This is also the window that was used to extract the line fluxes of all other lines (Table 2).

few stars in the immediate vicinity of the H II region, the higher estimate is likely more appropriate.

With the line flux measurements, we used two line ratio metrics to estimate the gas-phase oxygen abundance in BC6 (following Pettini & Pagel 2004), N2 = [N II]/Hα and O3N2 = ([O III]/Hβ)/([N II]/Hα). We note that these ratios are designed to be almost independent of our extinction correction, as [O III]$_{5007}$ and Hβ occur at almost the same wavelength, as do [N II]$_{6583}$ and Hα. We see (in Table 2) that both metrics give almost exactly the same oxygen abundance, despite each method having an intrinsic scatter of ∼0.2 dex.

Finally, we made a second estimate of the SFR based on the Hα line flux. Following the standard Kennicutt (1998) conversion, this equates to an SFR of $\log(\mathrm{SFR}_{\mathrm{H}\alpha}/M_\odot\ \mathrm{yr}^{-1}) = -4.36 \pm 0.13$.

4. Results

4.1. Morphology and Stellar Population

The optical appearance of BC6 is remarkably similar to that of BC4, which Jones et al. (2022b) concluded was likely in the process of becoming gravitationally unbound after losing its H I gas reservoir (presumably the majority of its initial total mass). Like BC4, BC6 is broken up into a few main components that are separated by tens of arcseconds (10″ = 800 pc at 16.5 Mpc). Each component contains multiple clumps of blue stars and has associated UV emission. In the HST image, these clumps of blue stars are partially resolved, with the brightest stars individually detected.

In the CMD of these resolved stars (Figure 4), we see a very similar stellar population to those of other blue blobs (Sand et al. 2017; Jones et al. 2022a, 2022b): a population of predominantly very blue (F606W–F814W = 0) stars and a second population at approximately F606W–F814W = 1. As in our previous works, we argue that this population is consistent with very young main-sequence stars and the blue and red sides of the helium-burning branch at the distance of the Virgo cluster (16.5 Mpc). The PAdova and TRieste Stellar Evolution Code (PARSEC; Bressan et al. 2012) isochrones overplotted in the middle panel of Figure 4 indicate that the entirety of the observed population is consistent with stars in the age range of 10–100 Myr. In particular, we point out that these isochrones were not fitted to the CMD in any way, yet the color range of the helium-burning stars in the isochrones matches closely with the observed color range. This range is mainly determined by the metallicity of the stars, which we independently measured (and input to the isochrones) from optical spectroscopy of the H II regions (Sections 3.5 and 4.2).

We also see no evidence of an old population in the form of a red giant branch (RGB). However, at the distance of Virgo, the tip of the RGB should occur at approximately F814W = 27 (Jang & Lee 2017), which is roughly the location of our 50% completeness limit. Even so, if a significant underlying old population were present, we would expect to see a buildup of RGB stars around the completeness limit. The absence of this population implies that BC6's stellar population is purely a young population; however, without deeper imaging, it is impossible to determine the exact age of the oldest stars.

The two SFR estimates (Table 1) from NUV and Hα differ by almost an order of magnitude. Although the HET observation only covered a single component of BC6, it was the main body (Figure 3, right), where most of the UV flux originates. As NUV is sensitive to SF over a longer timescale than Hα, this may be an indication that SF is currently ramping down in BC6. However, given the very low SFR in BC6, it is also possible that this is merely indicative of stochasticity in the number of high-mass stars produced in any given ∼10 Myr period.

4.2. Metallicity

Beccari et al. (2017) and Bellazzini et al. (2022) measured the metallicities of five blue blobs (SECCO 1, BC1, and BC3–5) using the same line ratio metrics as used here (see Section 3.5) and found a range of $8.29 < 12 + \log(\mathrm{O/H}) < 8.73$. BC6 fits

Table 2
Emission Line Fluxes and Metallicity Estimates of BC6

Hα	Hβ	[N II]$_{6583}$	[O III]$_{5007}$	12 + log(O/H)$_{\mathrm{N2}}$	12 + log(O/H)$_{\mathrm{O3N2}}$
168 ± 10	59 ± 14	38 ± 9	38 ± 12	8.53 ± 0.21	8.58 ± 0.25

Note. Line fluxes are in units of 10^{-18} erg s^{-1} cm^{-2} and are corrected for extinction.

comfortably within this range (8.58 ± 0.25). Thus, as with its stellar population, it seems quite consistent with the established sample of blue blobs.

Following the same rationale as Jones et al. (2022b), the above metallicity estimate implies that the progenitor galaxy of BC6 was likely in the stellar mass range $8.2 \lesssim \log(M_*/M_\odot) \lesssim 10.2$, assuming it roughly follows the mass–metallicity relation (Andrews & Martini 2013). The broad range is a reflection of the large uncertainty in the metallicity. Unfortunately, over this stellar mass range, the typical gas fraction ($M_{\mathrm{H\,I}}/M_*$) of a field galaxy smoothly transitions over the range $10 \gtrsim M_{\mathrm{H\,I}}/M_* \gtrsim 0.1$ (e.g., Huang et al. 2012); thus, the fact that BC6 is accompanied by $\sim 10^9\,M_\odot$ of H I gas does little to help narrow down the progenitor's stellar mass. However, it does mean that the progenitor must have lost a significant fraction, probably the majority, of its H I gas reservoir.

4.3. Stellar Mass

To estimate the stellar mass of BC6, we follow the same approach as Jones et al. (2022b); that is, we assume a constant SFR and continuously build up a synthetic stellar population (of matching metallicity) until the observed total F814W magnitude of BC6 is reached. Using this approach, we estimate a stellar mass of $\sim 2 \times 10^4\,M_\odot$, which at the observed (NUV-based) SFR could have been built up over approximately 80 Myr. If we instead use *g*- and *i*-band aperture photometry from the NGVS images and the scaling relations of Zibetti et al. (2009) and Taylor et al. (2011), we obtain estimates of 5×10^4 and $1 \times 10^5\,M_\odot$, respectively.

It is encouraging that all these estimates fall within a single order of magnitude, even if they still vary by a factor of 5. Although our initial estimate is smaller than both the others, we expect that this is the most representative of the actual stellar mass of BC6. Fundamentally, all three estimates rely on a mass-to-light scaling to produce a stellar mass, but only in our initial estimate is the synthetic population used to generate that mass-to-light ratio based on the observed metallicity and current SFR of BC6. This population is also quite atypical, with no apparent old population (older than a few hundred Myr); thus, standard scaling relations are unlikely to be entirely appropriate.

With a stellar mass of $2 \times 10^4\,M_\odot$, BC6 must have a gas fraction ($M_{\mathrm{H\,I}}/M_*$) of around 3000 if we only consider the gas in the coincident cloud (C3; Figure 3, left) or over 20,000 if we include the whole H I cloud complex. This makes it one of the most, if not the most, H I-rich extragalactic stellar systems known.

5. Discussion

5.1. Point of Origin

Although the stellar counterpart, BC6, was unknown until now, the origin of the H I cloud complex has been the subject of considerable discussion in the literature since it was first detected (Kent et al. 2007, 2009; Sorgho et al. 2017; Minchin et al. 2019). However, the gas-phase metallicity offers a new piece of pertinent information, and we also approach the question of the point of origin from a new standpoint in light of similar discussions for other blue blobs (Adams et al. 2015; Beccari et al. 2017; Sand et al. 2017; Bellazzini et al. 2018; Calura et al. 2020; Jones et al. 2022a, 2022b).

As mentioned by Minchin et al. (2019), tidal stripping does not seem to be a viable mechanism to form this structure. Not only is its isolation more difficult to explain with the low velocities ($\lesssim 300$ km s^{-1}) involved in tidal stripping (e.g., Bournaud & Duc 2006), but $10^9\,M_\odot$ represents a significant amount of H I gas for almost any galaxy, and it is not possible to tidally remove a large fraction of a galaxy's gas disk without also stripping stars. The exception to this would be if the progenitor was a particularly massive and H I-rich galaxy; however, that would also require a close passage from a similarly massive perturber to strip the gas, with neither remaining connected to the stripped gas in the present. Thus, the complete lack of stars over almost all of such a massive H I complex is a strong argument for ram pressure stripping, and we will only consider the formation of BC6 via this mechanism.

The H I cloud complex (Figure 3) is about 40′ across (∼190 kpc), making it plausible that the progenitor galaxy is a degree or more away. Unfortunately, despite there being no clear progenitor galaxy in the immediate vicinity of BC6, there are tens of potential parent objects that are Virgo members within a few degrees (Figure 6). Both Kent et al. (2009) and Minchin et al. (2019) focused on NGC 4445 and NGC 4424, as these are only ∼30′ to the SW of BC6 and have similar radial velocities to the gas complex (346 km s^{-1} and 437 km s^{-1}, respectively; Albareti et al. 2017; Haynes et al. 2018). NGC 4424 is in the process of being ram pressure stripped (Chung et al. 2009; Sorgho et al. 2017), but its H I tail points to the SE, roughly parallel to the H I complex containing BC6, rather than toward it. This makes NGC 4424 an unlikely point of origin of the H I complex. In the case of NGC 4445, the $M_{\mathrm{H\,I}}$–*B*-band diameter scaling relation of Jones et al. (2018) indicates that its expected original H I content (before falling into the Virgo cluster) would have been $\log M_{\mathrm{H\,I}}/M_\odot = 9.19 \pm 0.21$ (and it still contains $\log M_{\mathrm{H\,I}}/M_\odot = 7.7$; Haynes et al. 2018). The observed mass of the H I complex therefore represents almost its entire original H I content. In Sorgho et al. (2017, Figure A1), NGC 4445 also appears to have a ram pressure tail pointing away from the H I complex based on observations from the Karoo Array Telescope (KAT-7). However, Minchin et al. (2021) did not detect this tail in deep Arecibo observations, suggesting that it was likely an artifact in the KAT-7 data. Thus, NGC 4445 remains a possible point of origin, with the caveat that the H I mass of the complex represents virtually its entire original H I content.

In simulations of high-speed ram pressure stripping events (e.g., Kapferer et al. 2009; Tonnesen & Bryan 2012, 2021;

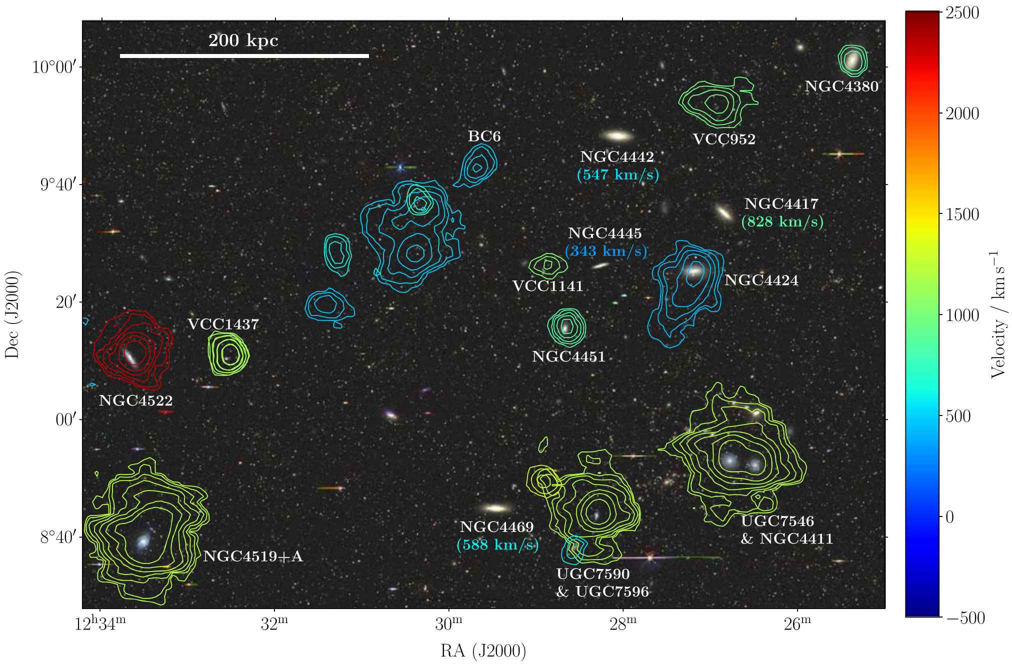

Figure 6. A wide-field DECaLS *grz* image showing the galaxies in the vicinity of BC6 and the H I complex. Contours showing H I emission from ALFALFA are overlaid (same contour levels as Figure 3). Each source identified by `SoFiA` is plotted separately, and the color of the contours corresponds to the flux-weighted mean velocity of each the source. Velocities for undetected sources are included as numerical values (from Cappellari et al. 2011; Albareti et al. 2017). We note that although NGC 4445 is weakly detected by ALFALFA (Haynes et al. 2018), it was not recovered in our automated extraction with `SoFiA`, as it has lost most of its H I.

Göller et al. 2023) on scales much larger than a galaxy, the tails that are formed are usually relatively linear features. This means that for progenitor candidates that are within ∼1° but not aligned with the major axis of the H I complex, a larger-than-expected opening angle would be required to explain the geometry of the structure. It would perhaps still be possible to reproduce the observed geometry by involving clumpy structure within the ICM (the simulations assume the ICM is uniform and moving at a constant velocity). However, in an attempt to narrow our focus to the most likely candidates, we will now consider potential progenitors that are roughly NW and SE of BC6, such that the cloud geometry can readily be explained by a simple ram pressure stripping scenario. There are six potentially viable progenitors within a few degrees: NGCs 4380, 4390, and 4442 to the NW and NGCs 4519, 4522, and 4535 to the SE. All are massive enough to meet the mass–metallicity requirement from Section 4.2, but three (NGCs 4380, 4442, and 4535) are actually above the expected mass range (stellar masses from Mosenkov et al. 2019). All except NGC 4442 currently contain some H I, detected in ALFALFA. The basic properties of these galaxies are summarized in Table 3.

We start by considering NGC 4442, as this is the closest major galaxy in projection (and velocity) along the direction of the major axis of the H I complex. This galaxy is undetected in ALFALFA, and its expected original H I content indicates that it has likely lost enough gas to account for the H I complex. However, this is also a relatively massive ($\log M_{*}/M_{\odot} = 10.6$; Mosenkov et al. 2019) and lenticular galaxy and has probably been without H I gas for some time. It seems quite improbable that a major stripping event could have occurred and NGC 4442 could have changed from a gas-rich galaxy to a quenched lenticular with no signs of the interaction in the time it took for the gas to move a few hundred kpc away. We therefore do not consider NGC 4442 a likely point of origin.

We see from the metallicity measurements (Table 3) that most of the galaxies with measurements could plausibly be matches for BC6 (Table 2), with only NGC 4390 being significantly disfavored because of its metallicity. The predicted original H I mass of NGC 4390 also suggests that it never would have had enough H I to form the cloud complex associated with BC6. Furthermore, it appears NGC 4390 has not lost a significant amount of H I.[19]

NGC 4380 was mapped in the VLA Imaging of Virgo in Atomic gas project (VIVA; Chung et al. 2009), which found that it has a truncated H I disk. This indicates a past episode of ram pressure stripping; however, the direction of stripping is unknown. This galaxy is also above the stellar mass range expected for the progenitor ($\log M_{*}/M_{\odot} = 10.4$; Mosenkov et al. 2019).

Unfortunately, VIVA did not map either NGC 4519 or NGC 4535. Both are detected in ALFALFA, but these data have an angular resolution of ∼4′. At this resolution, NGC 4535 appears undisturbed, but the H I distribution of NGC 4519 is clearly extended to the NW (toward BC6). However, NGC 4519 has a neighbor immediately to the NW (NGC 4519A) separated by only ∼200 km s^{-1} (Binggeli et al. 1985). Thus, the disturbance in the H I distribution of NGC 4519 may be the result of either tides or ram pressure, and with the resolution of the ALFALFA data, there is little chance of distinguishing the two.

NGC 4522 was mapped in VIVA and is a well-known example of a galaxy undergoing ram pressure stripping (e.g., Kenney & Koopmann 1999; Kenney et al. 2004; Vollmer et al. 2004; Chung et al. 2009). Furthermore, the direction of

---

[19] We note that the predicted original H I mass is usually intended as a statistical quantity and has considerable uncertainty for any individual galaxy. For example, the measured H I content of NGC 4519 *exceeds* its predicted original H I mass by over 0.1 dex. These values should be considered a rough guide only.

Table 3
Candidate Progenitor Galaxies for BC6

Galaxy (1)	v (km s^{-1}) (2)	Δv (km s^{-1}) (3)	Separation (4)	Direction (5)	$\log M_{\rm H\,I}$ (6)	$\log M_{\rm HI,pred}$ (7)	$\log M_{\rm HI,lost}$ (8)	12 + log(O/H) (9)
NGC 4380	963	463	79′	NW	8.51	9.40	9.34	⋯
NGC 4390	1101	601	86′	NW	8.68	8.85	8.36	8.37
NGC 4424	437	−63	47′	W	8.34	9.43	9.39	8.50
NGC 4442	547	47	37′	NW	<7.8	9.61	>9.60	⋯
NGC 4445	353	−147	31′	W	7.71	9.19	9.17	⋯
NGC 4519	1216	716	71′	SE	9.47	9.33	⋯	8.43
NGC 4522	2329	1819	54′	SE	8.66	9.45	9.37	8.45
NGC 4535	1963	1463	100′	SE	9.57	9.93	9.68	8.52

Note. Columns are as follows. (1) Galaxy name. (2) Heliocentric velocity from ALFALFA (Haynes et al. 2018). (3) Velocity difference between the galaxy and BC6 (Hα velocity). (4) Projected separation from the center of the H I complex (taken as the approximate midpoint between C1 and C4). (5) Approximate direction from the center of the H I complex to a given galaxy. (6) H I mass in ALFALFA (in $M_\odot$); typical uncertainties are 0.1 dex. NGC 4442 is undetected in ALFALFA, and we therefore use the 50% completeness limit (Haynes et al. 2011) and an assumed velocity width of 300 km s^{-1} to estimate an upper limit on its H I mass. (7) Predicted original H I mass in $M_\odot$ (Jones et al. 2018); the typical uncertainty is 0.21 dex. *B*-band diameters for the scaling relations were taken from de Vaucouleurs et al. (1991). (8) The predicted H I mass (in $M_\odot$) lost (i.e., the linear difference between columns (6) and (7)). (9) Metallicity measurements from De Vis et al. (2019); the typical uncertainty is 0.14 dex.

the stripping appears to be aligned along the direction toward BC6. However, BC6 and NGC 4522 are separated by ∼1800 km s^{-1} along the line of sight. Vollmer et al. (2006) attempted to simulate the gas stripping occurring in NGC 4522, finding that it was best fit by a very high velocity relative to the ICM (∼3500 km s^{-1}), with a velocity component in the SE direction of ∼3000 km s^{-1}. At this velocity, the distance between NGC 4522 and BC6 could be traversed in ∼100 Myr. Vollmer et al. (2006) estimate that the period of maximum stripping pressure on NGC 4522 was approximately 50 Myr ago. These two time frames do not exactly line up, but Vollmer et al. (2006) indicated that significant stripping is expected to begin well before the peak ram pressure is reached. With these high velocities, it may also be possible to explain the large velocity offset between BC6 and NGC 4522, if there is a significant component of NGC 4522's velocity (relative to the ICM) along the line of sight. Indeed, Minchin et al. (2019) identified a low column density extension of NGC 4522's ram pressure tail pointing in the direction of BC6 and the H I complex. Although this makes it tempting to conclude that the two are likely connected, this only extends about 5′ and 200 km s^{-1} toward the complex and therefore cannot be considered conclusive. Having said this, extrapolating this same velocity gradient another ∼40′ would bring us to both the approximate position and velocity of the H I complex.

Another point in favor of NGC 4522 is that ram pressure stripping simulations (e.g., Tonnesen & Bryan 2012; Lee et al. 2022) show that most SF in stripped gas occurs either in the immediate vicinity of the galaxy or in the distant extremity of the tail. As BC6 is the only apparent stellar counterpart of the entire H I complex (see Appendix) and is at the NW end of the tail, to be consistent with these simulations, we would expect the point of origin to be to the SE, which NGC 4522 is.

Minchin et al. (2019) consider NGC 4522 as a possible progenitor but reject it on a couple of grounds. First, they argue that if the H I complex originated from NGC 4522, then one might expect cloud C5 to be at a higher radial velocity than C3 (see Figure 3) because it is closer to NGC 4522, but the reverse is true. However, the velocity dispersion of the whole structure is quite low, and such an inconsistency might be explained by the two clouds being stripped from different sides of the galaxy (thus having different initial velocities). Also, the initial velocity relative to the ICM would be rapidly reduced; thus, the original objection may not be valid if the H I complex has been separated from NGC 4522 for long enough for the entire structure to come to rest relative to the ICM.

The second issue raised by Minchin et al. (2019) is that it is unlikely that the local ICM radial velocity in this region of Virgo is as low as 500 km s^{-1} (recall that in Section 2 we mentioned that the typical velocity of galaxies in this region of Virgo is ∼1000 km s^{-1}). If this is not the case, then it is not plausible that the H I gas could have initially had a radial velocity of ∼2300 km s^{-1} and then slowed to ∼500 km s^{-1}. This is a more serious objection to NGC 4522 as the progenitor and is difficult to dismiss. The ram pressure stripping simulations of Vollmer et al. (2006) are best able to reproduce the extraplanar gas distribution of NGC 4522 with an incidence angle of about 60° between the galaxy's motion and the ICM's. However, in this configuration, the radial velocity of the ICM would be approximately 1000 km s^{-1}. An ICM velocity as low as 500 km s^{-1} could be possible in different configurations, but Vollmer et al. (2006) found that such configurations would not reproduce the observed gas distribution. We note that a similar (though less severe) objection regarding the ICM velocity applies to all the candidate progenitor galaxies to the NW and SE listed in Table 3, as these all have radial velocities above 500 km s^{-1}. If one of these is indeed the origin of BC6, then this may be an indication that we do not understand the motions (and perhaps, substructure) of the ICM in this region of Virgo, and it might be necessary to revisit the hydrodynamical modeling of the gas stripping in NGC 4522 to determine if other factors such as irregular motions and clumpiness in the ICM could reconcile these differences.

Finally, Minchin et al. (2019) noted that the apparent gap in H I between the ram pressure tail still connected to NGC 4522 and the H I complex around BC6 would require two stripping episodes, with a break in between. However, simulations such as Kapferer et al. (2009) and Tonnesen & Bryan (2012) show similar morphology, with significant gaps in the H I column density of the tails despite continuous stripping. Gas that is initially heated (and therefore not visible in 21 cm line emission) may cool and condense back into H I clouds in the tail, especially if the gas is metal-rich (e.g., Lee et al. 2022). However, it is not clear if this is a viable mechanism for such a large quantity of gas as is associated with BC6.

To summarize, we have considered a number of potential progenitor galaxies within a few degrees of BC6, but there is no clear parent object; in fact, all the candidates appear to have at least one disqualifying factor. We consider NGC 4522 to be the most likely parent object because it has similar metallicity and is a known case of extreme ram pressure stripping with the gas tail pointing toward BC6 in both projection and velocity. However, it is difficult to account for the kinematic separation of NGC 4522 and BC6. NGC 4380 and NGC 4519 also remain candidates for the progenitor, but this may simply be because there are fewer observations of these galaxies, and we could be ignorant of disqualifying information. NGC 4445 was suggested as the point of origin by Kent et al. (2009) and Minchin et al. (2019); however, we slightly disfavor this galaxy as the progenitor, as the observed H I complex represents almost the entirety of its estimated original gas content, and the ram pressure tail would need a particularly wide opening angle to explain the extent of the complex.

5.2. Fate

Here we briefly consider the evaporation timescale for the clouds seen in the H I complex as a means to determine the fate of BC6. Following the discussion of Borthakur et al. (2010), which itself is based on Cowie & McKee (1977) and Vollmer et al. (2001), we see that cloud evaporation can proceed in either the classical or saturation scenario depending on the value of σ_0, the ratio of the classical and saturated heat flux through the spherical shell of the cloud, where

$$\sigma_0 \approx \frac{(T_{\rm ICM}/1 \times 10^7\ {\rm K})^2}{n_{\rm ICM} R_{\rm cloud}}, \tag{1}$$

and $T_{\rm ICM}$ is the temperature of the hot ICM, $n_{\rm ICM}$ is its number density (in cm^{-3}), and $R_{\rm cloud}$ is the cloud radius (in pc). To evaluate this and proceed, we need to know the physical properties of both a cloud within the H I complex and the surrounding ICM.

To obtain the approximate physical properties of a single cloud (as far as possible), we take the values for C2 (Figure 3, left), which was observed with the VLA in Kent et al. (2009). In this higher-resolution imaging, the cloud has an elongated structure with two main concentrations of mass. For simplicity, we take a quarter of the H I major axis ($1\rlap{.}'5$) measured as the radius of a single cloud (~2 kpc) and half of the total H I mass of C2 as its mass ($2.6 \times 10^7\ M_\odot$). Here we have also multiplied by 1.4 to account for helium and other metals. Assuming a spherical geometry gives a cloud number density of ~0.3 cm^{-3}.

For the ICM properties, we use the simple β-model ICM density profile used in Vollmer et al. (2001), evaluated at $2\rlap{.}^\circ7$ (the separation between BC6 and M87), to obtain an ICM density estimate of 10^{-4} cm^{-3}. For the temperature, we see from the profile plotted by Böhringer et al. (1994) that at $2\rlap{.}^\circ7$ from M87, the average temperature of the ICM is roughly 2 keV (1.5×10^7 K).

Using the above values in Equation (1), we see that this cloud is in the saturated regime (i.e., $\sigma_0 > 1$), where the evaporation speed is limited by the rate heat can be conducted through the shell of the cloud. The expression derived by Borthakur et al. (2010) for the lifetime of an H I cloud in this regime is

$$\tau \approx \frac{n_{\rm cloud} R_{\rm cloud}}{n_{\rm ICM} \sqrt{T_{\rm ICM}}}\ {\rm Myr}, \tag{2}$$

where $n_{\rm cloud}$ is the average number density of the cloud (in cm^{-3}). The other quantities are the same as in Equation (1). Evaluating this expression gives a cloud lifetime for C2 of over a Gyr.

Although this is only an order-of-magnitude estimate, it is clear from the stellar population (Section 4.1) that the H I complex has been traversing the ICM for at least ~100 Myr and is still an extremely rich H I structure. Furthermore, Calura et al. (2020) considered in detail the survival of a much smaller gas cloud, $M_{\rm H\,I} \sim 10^7\ M_\odot$ (designed to mimic SECCO 1), finding that when simulating it traversing the ICM at high speed, it could still survive as a distinct structure for around a Gyr. Thus, given the enormous reservoir still present, it seems that BC6 is not in imminent danger of losing its H I gas and is unlikely to become unbound and disperse into the cluster in the short term.

However, as the H I complex will not have significant dark matter content, it unquestionably cannot survive indefinitely in the Virgo cluster. On long timescales, it will eventually evaporate, and its aging stars will disperse and contribute to the intracluster light. Indeed, a Gyr is on the order of the orbital timescale of the cluster; thus, it is possible that the complex would undergo interactions with inhomogeneities in the ICM within that time or, given its scale, might experience a strong tidal interaction with a galaxy, either of which could act to disperse it and shorten its expected lifetime. In addition, if SF continues, then stellar feedback may also act to disperse the structure, especially as it is not supported by the additional potential well of a dark matter halo. Thus, the evaporation timescale is likely an upper limit on how long this structure can survive, even if individual clouds might in theory survive that long.

6. Conclusions

We have identified the stellar counterpart (BC6) of an enormous, isolated H I structure (~190 kpc long, $M_{\rm H\,I} \sim 10^9\ M_\odot$) in the Virgo cluster that has been thought to be "dark" since its discovery by Kent et al. (2007). The extremely low (stellar) mass counterpart lies at the NW tip of the structure (Figure 3). In ground-based imaging, it appears as faint and irregular blue clumps, which HST images reveal to consist exclusively of young ($\lesssim$100 Myr) stars. Given this population, the total stellar mass of BC6 is likely only a few times $10^4\ M_\odot$, making it a truly extreme object in terms of gas fraction.

An optical spectrum of this counterpart from HET returned an Hα redshift (500 km s^{-1}) consistent with the velocity of the cospatial H I gas seen in ALFALFA and with GBT observations, thereby confirming association. This spectrum also revealed that BC6 is metal-rich (given its low stellar mass), indicating that its gas complex must have originated in a galaxy where the gas could be preenriched.

Given these properties, BC6 appears to be a member of the novel stellar systems described by Jones et al. (2022b), known as "blue blobs," standing out only because of its extraordinary H I content. The origin of this gas is as challenging to conclusively determine as are the origins of previously studied blue blobs. However, high-speed ram pressure stripping remains the most plausible explanation, regardless of which cluster member was the origin. We favor NGC 4522 as a candidate point of origin as it has a similar metallicity, is a known example of ongoing extreme ram pressure stripping, and probably passed through the local peak of X-ray emission (from the ICM), where BC6 currently resides, about 100 Myr ago (Böhringer et al. 1994; Vollmer et al. 2001). However, this association is far from conclusive; in particular, the kinematic separation of BC6 and NGC 4522 is difficult to explain.

Given how long this H I structure was known without a stellar counterpart being discovered, it seems likely other “dark” H I structures in Virgo (e.g., Kent et al. 2007; Taylor et al. 2012) may host similarly faint blue blob counterparts as well. This is a possibility that we aim to investigate through our ongoing citizen science search covering the entire cluster.

Acknowledgments

We thank the anonymous referee for the constructive comments that helped to improve this work. We gratefully acknowledge the work of all the Zooniverse volunteers who have participated in the Blobs and Blurs project. This publication uses data generated via the Zooniverse.org platform, development of which is funded by generous support, including a Global Impact Award from Google, and by a grant from the Alfred P. Sloan Foundation. This work is based on observations made with the NASA/ESA Hubble Space Telescope, obtained at the Space Telescope Science Institute, which is operated by the Association of Universities for Research in Astronomy, Inc., under NASA contract NAS5-26555. These observations are associated with program No. HST-GO-17267. Support for program No. HST-GO-17267 was provided by NASA through a grant from the Space Telescope Science Institute. D.J.S. and the Arizona team acknowledge support from NSF grant AST-2205863, as well as support through the Arizona NASA Space Grant Consortium, Cooperative Agreement 80NSSC20M0041. K.S. acknowledges support from the Natural Sciences and Engineering Research Council of Canada (NSERC). D.C. acknowledges support from NSF grant AST-1814208. A.K. acknowledges support from NSERC, the University of Toronto Arts & Science Postdoctoral Fellowship program, and the Dunlap Institute. We acknowledge the Texas Advanced Computing Center (TACC) at the University of Texas at Austin for providing high-performance computing, visualization, and storage resources that have contributed to the results reported within this paper. This work used images from the Dark Energy Camera Legacy Survey (DECaLS; Proposal ID 2014B-0404; PIs: David Schlegel and Arjun Dey). Full acknowledgment is at https://www.legacysurvey.org/acknowledgment/. This research used the facilities of the Canadian Astronomy Data Centre operated by the National Research Council of Canada with the support of the Canadian Space Agency. The Green Bank Observatory is a facility of the National Science Foundation operated under cooperative agreement by Associated Universities, Inc. The National Radio Astronomy Observatory is a facility of the National Science Foundation operated under cooperative agreement by Associated Universities, Inc.

Facilities: HST(ACS), GBT, HET, Arecibo, CFHT, Blanco, GALEX.

Software: `DOLPHOT`[20](Dolphin 2000, 2016), `SoFiA`[21] (Serra et al. 2014, 2015), `astropy`[22] (Astropy Collaboration et al. 2013, 2018), `reproject`[23] (Robitaille et al. 2020), `DS9`[24] (Joye & Mandel 2003), `Aladin`[25] (Bonnarel et al. 2000; Boch & Fernique 2014), `CASA`[26] (McMullin et al. 2007), `GBTIDL`[27], `dustmaps`[28] (Green 2018), `matplotlib`[29] (Hunter 2007), `numpy`[30] (van der Walt et al. 2011), `scipy`[31] (Oliphant 2007; Millman & Aivazis 2011), `pandas`[32] (pandas development team, T 2020; McKinney 2010), `Panacea`[33], `LRS2Multi`[34], `dust_extinction`.[35]

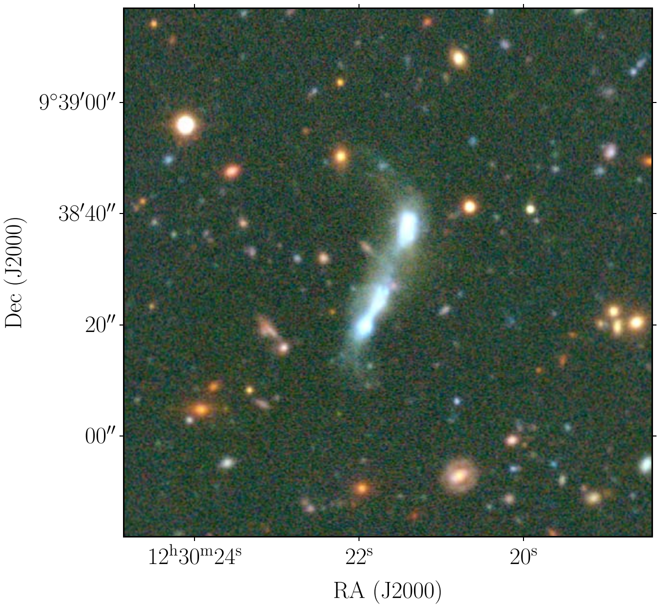

Figure 7. NGVS *ugi* image of an additional blue blob candidate cospatial with H I cloud C4 (Figure 3) identified in our citizen science search. However, this candidate appears to be background galaxies.

Appendix
Other Counterpart Candidates

Our citizen science search for additional blue blob candidates throughout Virgo was recently completed. We extracted all the candidates in this region to identify if BC6 is the only object associated with the H I tail or if there might be other candidate blue blobs coincident with other clouds.

We only found one additional candidate (Figure 7) coincident with the H I structure, next to cloud C4 (Figure 3). The appearance of this candidate suggests that it is likely a background group of interacting galaxies. Although there are blue clumps, as in genuine blue blobs, they are surrounded by diffuse yellow light, probably made up of old stars that are very far away. Thus, we do not consider this likely to be a genuine blue blob or associated with the H I structure; however,

---

[20] http://americano.dolphinsim.com/dolphot/

[21] https://gitlab.com/SoFiA-Admin/SoFiA

[22] https://www.astropy.org/index.html

[23] https://reproject.readthedocs.io/en/stable/

[24] https://sites.google.com/cfa.harvard.edu/saoimageds9

[25] https://aladin.u-strasbg.fr/

[26] https://casa.nrao.edu/

[27] https://gbtidl.nrao.edu/

[28] https://dustmaps.readthedocs.io/en/latest/

[29] https://matplotlib.org/

[30] https://numpy.org/

[31] https://scipy.org/

[32] https://pandas.pydata.org/

[33] https://github.com/grzeimann/Panacea

[34] https://github.com/grzeimann/LRS2Multi

[35] https://dust-extinction.readthedocs.io

we plan to obtain optical spectroscopic follow-up in the future to rule this out.

ORCID iDs

Michael G. Jones https://orcid.org/0000-0002-5434-4904
Steven Janowiecki https://orcid.org/0000-0001-9165-8905
Swapnaneel Dey https://orcid.org/0009-0006-0732-3031
David J. Sand https://orcid.org/0000-0003-4102-380X
Paul Bennet https://orcid.org/0000-0001-8354-7279
Denija Crnojević https://orcid.org/0000-0002-1763-4128
Catherine E. Fielder https://orcid.org/0000-0001-8245-779X
Ananthan Karunakaran https://orcid.org/0000-0001-8855-3635
Brian R. Kent https://orcid.org/0000-0002-8990-1811
Nicolas Mazziotti https://orcid.org/0009-0005-9612-4722
Burçin Mutlu-Pakdil https://orcid.org/0000-0001-9649-4815
Kristine Spekkens https://orcid.org/0000-0002-0956-7949

References

Adams, E. A. K., Cannon, J. M., Rhode, K. L., et al. 2015, A&A, 580, A134
Adams, E. A. K., Giovanelli, R., & Haynes, M. P. 2013, ApJ, 768, 77
Albareti, F. D., Allende Prieto, C., Almeida, A., et al. 2017, ApJS, 233, 25
Andrews, B. H., & Martini, P. 2013, ApJ, 765, 140
Astropy Collaboration, Price-Whelan, A. M., Sipőcz, B. M., et al. 2018, AJ, 156, 123
Astropy Collaboration, Robitaille, T. P., Tollerud, E. J., et al. 2013, A&A, 558, A33
Beccari, G., Bellazzini, M., Magrini, L., et al. 2017, MNRAS, 465, 2189
Bellazzini, M., Armillotta, L., Perina, S., et al. 2018, MNRAS, 476, 4565
Bellazzini, M., Magrini, L., Jones, M. G., et al. 2022, ApJ, 935, 50
Bellazzini, M., Magrini, L., Mucciarelli, A., et al. 2015, ApJL, 800, L15
Binggeli, B., Sandage, A., & Tammann, G. A. 1985, AJ, 90, 1681
Binggeli, B., Tammann, G. A., & Sandage, A. 1987, AJ, 94, 251
Boch, T., & Fernique, P. 2014, in ASP Conf. Ser. 485, Astronomical Data Analysis Software and Systems XXIII, ed. N. Manset & P. Forshay (San Francisco, CA: ASP), 277
Böhringer, H., Briel, U. G., Schwarz, R. A., et al. 1994, Natur, 368, 828
Bonnarel, F., Fernique, P., Bienaymé, O., et al. 2000, A&AS, 143, 33
Borthakur, S., Yun, M. S., & Verdes-Montenegro, L. 2010, ApJ, 710, 385
Bournaud, F., & Duc, P. A. 2006, A&A, 456, 481
Bradley, L., Sipőcz, B., Robitaille, T., et al. 2020, astropy/photutils: v1.0.0, Zenodo, doi:10.5281/zenodo.4044744
Bressan, A., Marigo, P., Girardi, L., et al. 2012, MNRAS, 427, 127
Burkhart, B., & Loeb, A. 2016, ApJL, 824, L7
Calura, F., Bellazzini, M., & D'Ercole, A. 2020, MNRAS, 499, 5873
Cappellari, M., Emsellem, E., Krajnović, D., et al. 2011, MNRAS, 413, 813
Chengalur, J. N., Giovanelli, R., & Haynes, M. P. 1995, AJ, 109, 2415
Chonis, T. S., Hill, G. J., Lee, H., et al. 2016, Proc. SPIE, 9908, 99084C
Chung, A., van Gorkom, J. H., Kenney, J. D. P., Crowl, H., & Vollmer, B. 2009, AJ, 138, 1741
Cowie, L. L., & McKee, C. F. 1977, ApJ, 211, 135
Davies, J., Minchin, R., Sabatini, S., et al. 2004, MNRAS, 349, 922
de Vaucouleurs, G., de Vaucouleurs, A., Corwin, H. G., Jr., et al. 1991, Third Reference Catalogue of Bright Galaxies. Volume I: Explanations and references. Volume II: Data for galaxies between 0^h and 12^h. Volume III: Data for galaxies between 12^h and 24^h (New York: Springer)
De Vis, P., Jones, A., Viaene, S., et al. 2019, A&A, 623, A5
Dey, A., Schlegel, D. J., Lang, D., et al. 2019, AJ, 157, 168
Dolphin, A., 2016 DOLPHOT: Stellar photometry, Astrophysics Source Code Library, ascl:1608.013
Dolphin, A. E. 2000, PASP, 112, 1383
Ferrarese, L., Côté, P., Cuillandre, J.-C., et al. 2012, ApJS, 200, 4
Fitzpatrick, E. L. 2004, ASP Conf. Ser. 309, Astrophysics of Dust, ed. A. N. Witt, G. C. Clayton, & B. T. Draine (San Francisco, CA: ASP), 33
Giovanelli, R., & Haynes, M. P. 1989, ApJL, 346, L5
Giovanelli, R., Haynes, M. P., Kent, B. R., et al. 2005, AJ, 130, 2598
Göller, J., Joshi, G. D., Rohr, E., Zinger, E., & Pillepich, A. 2023, MNRAS, 525, 3551
Green, G. M. 2018, JOSS, 3, 695
Haynes, M. P., Giovanelli, R., & Kent, B. R. 2007, ApJL, 665, L19
Haynes, M. P., Giovanelli, R., Kent, B. R., et al. 2018, ApJ, 861, 49
Haynes, M. P., Giovanelli, R., Martin, A. M., et al. 2011, AJ, 142, 170
Hill, G. J., Lee, H., MacQueen, P. J., et al. 2021, AJ, 162, 298
Huang, S., Haynes, M. P., Giovanelli, R., & Brinchmann, J. 2012, ApJ, 756, 113
Hunter, J. D. 2007, CSE, 9, 90
Iglesias-Páramo, J., Buat, V., Takeuchi, T. T., et al. 2006, ApJS, 164, 38
Jang, I. S., & Lee, M. G. 2017, ApJ, 835, 28
Jones, M. G., Papastergis, E., Pandya, V., et al. 2018, A&A, 614, A21
Jones, M. G., Sand, D. J., Bellazzini, M., et al. 2022a, ApJL, 926, L15
Jones, M. G., Sand, D. J., Bellazzini, M., et al. 2022b, ApJ, 935, 51
Jones, M. G., Verdes-Montenegro, L., Moldon, J., et al. 2023, A&A, 670, A21
Joye, W. A., & Mandel, E. 2003, in ASP Conf. Ser. 295, Astronomical Data Analysis Software and Systems XII, ed. H. E. Payne, R. I. Jedrzejewski, & R. N. Hook (San Francisco, CA: ASP), 489
Józsa, G. I. G., Jarrett, T. H., Cluver, M. E., et al. 2022, ApJ, 926, 167
Kapferer, W., Sluka, C., Schindler, S., Ferrari, C., & Ziegler, B. 2009, A&A, 499, 87
Karunakaran, A., & Spekkens, K. 2024, RNAAS, 8, 24
Kenney, J. D. P., & Koopmann, R. A. 1999, AJ, 117, 181
Kenney, J. D. P., van Gorkom, J. H., & Vollmer, B. 2004, AJ, 127, 3361
Kennicutt, R. C., Jr. 1998, ARA&A, 36, 189
Kent, B. R., Giovanelli, R., Haynes, M. P., et al. 2007, ApJL, 665, L15
Kent, B. R., Spekkens, K., Giovanelli, R., et al. 2009, ApJ, 691, 1595
Laher, R. R., Gorjian, V., Rebull, L. M., et al. 2012, PASP, 124, 737
Lee, J., Kimm, T., Blaizot, J., et al. 2022, ApJ, 928, 144
Martin, D. C., Fanson, J., Schiminovich, D., et al. 2005, ApJL, 619, L1
McKinney, W. 2010, in Proc. 9th Python in Science Conf., ed. S. van der Walt & J. Millman, 56
McMullin, J. P., Waters, B., Schiebel, D., Young, W., & Golap, K. 2007, ASP Conf. Ser. 376, Astronomical Data Analysis Software and Systems XVI, ed. R. A. Shaw, F. Hill, & D. J. Bell, 127
Mei, S., Blakeslee, J. P., Côté, P., et al. 2007, ApJ, 655, 144
Millman, K. J., & Aivazis, M. 2011, CSE, 13, 9
Minchin, R., Davies, J., Disney, M., et al. 2005, ApJL, 622, L21
Minchin, R., Taylor, R., & Deshev, B. 2021, RNAAS, 5, 217
Minchin, R. F., Taylor, R., Köppen, J., et al. 2019, AJ, 158, 121
Morrissey, P., Conrow, T., Barlow, T. A., et al. 2007, ApJS, 173, 682
Mosenkov, A. V., Baes, M., Bianchi, S., et al. 2019, A&A, 622, A132
Oliphant, T. E. 2007, CSE, 9, 10
O'Neil, K., van Driel, W., & Schneider, S. 2024, AAS Meeting Abstracts, 56, 404.13
Osterbrock, D. E. 1989, Astrophysics of Gaseous Nebulae and Active Galactic Nuclei (Melville, NY: Univ. Science Books)
pandas development team, T 2020, pandas-dev/pandas: Pandas, v1.2.5, Zenodo, doi:10.5281/zenodo.3509134
Pettini, M., & Pagel, B. E. J. 2004, MNRAS, 348, L59
Ramsey, L. W., Adams, M. T., Barnes, T. G., et al. 1998, Proc. SPIE, 3352, 34
Robitaille, T., Deil, C., & Ginsburg, A., 2020 reproject: Python-based astronomical image reprojection, Astrophysics Source Code Library, ascl:2011.023
Sand, D. J., Crnojević, D., Bennet, P., et al. 2015, ApJ, 806, 95
Sand, D. J., Seth, A. C., Crnojević, D., et al. 2017, ApJ, 843, 134
Schlafly, E. F., & Finkbeiner, D. P. 2011, ApJ, 737, 103
Schlegel, D. J., Finkbeiner, D. P., & Davis, M. 1998, ApJ, 500, 525
Serra, P., Westmeier, T., Giese, N., et al., 2014 SoFiA: Source Finding Application, Astrophysics Source Code Library, ascl:1412.001
Serra, P., Westmeier, T., Giese, N., et al. 2015, MNRAS, 448, 1922
Sirianni, M., Jee, M. J., Benítez, N., et al. 2005, PASP, 117, 1049
Sorgho, A., Hess, K., Carignan, C., & Oosterloo, T. A. 2017, MNRAS, 464, 530
Taylor, E. N., Hopkins, A. M., Baldry, I. K., et al. 2011, MNRAS, 418, 1587
Taylor, R., Davies, J. I., Auld, R., & Minchin, R. F. 2012, MNRAS, 423, 787
Tonnesen, S., & Bryan, G. L. 2012, MNRAS, 422, 1609
Tonnesen, S., & Bryan, G. L. 2021, ApJ, 911, 68
van der Walt, S., Colbert, S. C., & Varoquaux, G. 2011, CSE, 13, 22
Verdes-Montenegro, L., Yun, M. S., Williams, B. A., et al. 2001, A&A, 377, 812
Vollmer, B., Beck, R., Kenney, J. D. P., & van Gorkom, J. H. 2004, AJ, 127, 3375
Vollmer, B., Cayatte, V., Balkowski, C., & Duschl, W. J. 2001, ApJ, 561, 708
Vollmer, B., Soida, M., Otmianowska-Mazur, K., et al. 2006, A&A, 453, 883
Wong, O. I., Stevens, A. R. H., For, B. Q., et al. 2021, MNRAS, 507, 2905
Wyder, T. K., Martin, D. C., Schiminovich, D., et al. 2007, ApJS, 173, 293
Zhou, R., Zhu, M., Yang, Y., et al. 2023, ApJ, 952, 130
Zibetti, S., Charlot, S., & Rix, H.-W. 2009, MNRAS, 400, 1181